High Performance Organic Transistors Using Small Molecule Semiconductors and High Permittivity Semiconducting Polymers

Keri L. McCall, Simon R. Rutter, Elizabeth L. Bone, Neil D. Forrest, James S. Bissett, Julie D. E. Jones, Michael J. Simms, Aaron J. Page, Raymond Fisher, Beverley A. Brown, and Simon D. Ogier*

High mobility organic semiconductor formulations with excellent uniformity across large area substrates are prepared via the use of formulations containing small molecule and high permittivity semiconducting oligomers. The use of these high-*k* ($k > 3.3$) oligomers allows control of the wetting via the manipulation of the surface energy of the substrate being coated. Organic thin film transistors results with mobilities of up to 5 $cm^2 V^{-1} s^{-1}$, standard deviation <10 %, on/off ratios of 10^9 are presented.

1. Introduction

Organic thin film transistors (OTFT) have been studied extensively as a technology that is applicable to backplanes used in flexible display applications. Charge mobility values for evaporated and solution processed materials have already exceeded those of amorphous silicon. A recent review concluded that by mid 2011 there were approximately 40 organic semiconductor (OSC) materials reported in the literature having charge mobilities >1 $cm^2 V^{-1} s^{-1}$.[1] Despite this wide range of OSC materials, there have been only a few practical demonstrations of the large scale integration of OTFTs, or the use of these high performance materials in display backplanes.[2–4] The OTFTs demonstrated in practical applications have mainly been evaporated small molecule OSCs such as pentacene and PXX (peri-xanthenoxanthone).[5] However, the evaporation approach is unsuitable for industrial manufacture of OTFT backplanes because it is difficult to control the uniformity of the crystalline OSC on large substrates. For this reason, solution processed OSCs are favored. In addition solution processing has the potential to be lower cost due to the omission of the lengthy vacuum process required to deposit OSC materials by evaporation and has the potential to benefit from a direct printing technique such as ink jet or flexo/gravure.

The use of formulated small molecule semiconductors in combination with polymer binders and suitable solvents are already well known in the field of organic electronics.[6,7] These OSC formulations have been used in the past to yield uniform thin films by spin coating onto large area substrates. Earlier studies have limited themselves to reporting the performance data from small molecule/binder formulations wherein the binder is a low permittivity semiconducting or insulating binder.[8] For the purpose of this study, polymer binders having a permittivity, ε or k (at 1000 Hz), of ≤3.3 are considered to be low permittivity polymers (the so called low-*k* binders) and polymers having permittivity values >3.3 are considered to be high permittivity (the so-called high-*k* binders). In this study, semiconducting binders have been synthesized having permittivities ranging from 2.6 up to 4.6 and these have been formulated with a high performance small molecule semiconductor, 1,4,8,11-tetramethyl-6,13-bis(triethylsilylethynyl) pentacene (hereafter referred to as TMTES).[9] It has been found that the permittivity of the binder is a key factor in controlling the phase separation of the small molecule within the resulting OSC layer which in turn has a significant impact on the resulting mobility and uniformity of the OSC in the OTFT. This can be heavily influenced by the surface energy of the substrate onto which the OSC formulation is deposited, which in turn influences the small molecule/binder phase separation. The control of the phase separation is important due to the effect that this has on the overall device performance and wet film stability during coating. Ideally the small molecule should be present in a well ordered layer at the dielectric interface (in top gate architecture this is the air interface during coating) as this creates a high mobility charge transport channel.[10] If the phase separation is non-ideal then the active interface can be a mixed phase with poor molecular ordering of the small molecule, resulting in poorer charge transport and lower mobility OTFT devices.[11] In addition, the improved ordering of the small molecule has been shown in some cases also to improve the thermal stability of the OSC

Dr. K. L. McCall, Dr. S. R. Rutter, E. L. Bone,
Dr. B. A. Brown, Dr. S. D. Ogier
Centre for Process Innovation
National Printable Electronics Centre
Thomas Wright Way, NetPark, Sedgefield TS21 3FG, UK
E-mail: Keri.McCall@uk-cpi.com
Dr. N. D. Forrest, Dr. J. S. Bissett, Dr. J. D. E. Jones,
Dr. M. J. Simms, A. J. Page, Dr. R. Fisher
Peakdale Molecular Ltd.
Peakdale Science Park
Sheffield Road, Chapel-en-le-Frith, High Peak SK23 0PG, UK

DOI: 10.1002/adfm.201303336

thin film.[12,13] The main approaches used to influence the performance of the OSC blends have focused on polymer attributes such as molecular weight, polymer to small molecule ratio in the formulation and most recently hydrophobicity of the polymer. To date there have been no studies combining surface energy of the substrate and polarity of the polymer to enable control of the thin film formation. Using the aim of improved phase separation via a controllable process parameter, as outlined in this paper, it has been shown that the use of a high-*k* binder can achieve this in combination with the performance attributes of high mobility and good uniformity (<10% standard deviation in charge mobility) of the OTFTs across a 4 × 4 inch substrate can be achieved simultaneously. Furthermore, the channel length dependence of the mobility, a well recognized industry problem[6] has been shown to be minimized for these formulations.

In this paper novel small molecule/binder formulations having linear mobility of ≈5 cm^2 V^{-1} s^{-1} achieved at operating voltages of <10 V are presented. These materials can be processed at low temperatures from solution and coated over large areas. This high performance at low gate voltage has the potential to be useful in a range of applications such as flexible display backplanes or low cost kHz frequency printed logic applications.

2. Effects of Manufacturing

Manufacture of electronics on a large scale is a well established industry having excellent control of repeatability and high yields.[14] If organic electronics, such as OTFTs, are to be successfully adopted by and integrated into this industry then consideration of the likely process conditions needs to be made and all of the component materials of the OTFT optimized with this in mind, not least the OSC. For example, it is common practice to remove organic contamination from substrates using argon, oxygen and/or ozone plasma treatment prior to depositing subsequent layers in the transistor device.[15] This is necessary to remove any unwanted organic residue on the surface, improving the yield and uniformity of the array. Another common process used in industrial manufacture of display backplanes is the sputter deposition of contact metals and subsequent patterning, typically using strong oxidizers such as nitric acid. For TFT backplanes these scalable processes are preferred compared to techniques such as evaporation due to the requirement for high uniformity and repeatability across large areas. These industrial process techniques will result in the formation of a surface with a high polar component of the surface free energy, even if a non-polar planarizing layer has been originally deposited. We have used the negative photo-resist SU8 (Microchem Corp.) as a planarizing material and it is deposited immediately below the OSC layer, **Figure 1**.

Table 1 shows the results of the surface free energy (SFE) measurements of SU8-2002 that were obtained after several typical TFT fabrication process steps. It shows that there is an increase in the polar component of the SFE of the SU8-2002 following sputtering and plasma treatment. This is most probably due to the formation of polar, oxygen-containing species on the SU8-2002 surface.[16] AFM studies conducted in this work of the SU8-2002 surface after each process step show an increased surface roughness effect, (refer to **Table 2**). Whilst the surface energy and roughness of the planarizer layers can be modified after these fabrication steps, potentially through the use of self-assembled monolayers (SAMs), it is likely that the SAM treatment could also affect the electrode to OSC interface thereby making charge injection less efficient. Therefore OSC layers that do not require these additional process steps or monolayers to achieve high performance on polar surfaces are very desirable.

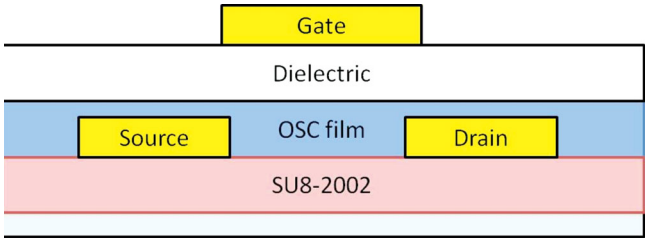

Figure 1. Top gate, bottom contact device architecture with SU8-2002 acting as a planarizing layer for the carrier substrate.

3. Materials Development

To investigate whether the polar surfaces generated by these standard fabrication processes affected the OSC formulation performance, a range of semiconducting binder materials were prepared (**Figure 2**). These materials have permittivity values ranging from 2.6 to 4.6, and were extensively purified to minimise trace contaminant levels.

The copolymer of 4-(*sec*-butyl) triarylamine and tetraoctylindenofluorene **1** and 2,4-dimethylpolytriarylamine **2** were prepared according to previously published procedures[17,18] and copolymer **5** was prepared in an analogous manner to **1**. Further details of the synthesis can be found in the Supporting Information.

The novel semiconducting binder **3**, prepared following a similar procedure to **2**, was found to have very high permittivity

Table 1. Summary of surface free energy of SU8-2002 after OTFT process fabrication steps.

SFE [mN m^{-1}]	SU8 as cured	SU8 after Au sputter deposition	SU8 after Ar/O_2 plasma
Dispersive	34.1	45.2	44.7
Polar	5.4	20.0	33.7
Total	39.5	65.2	78.4

Table 2. Surface roughness of SU8-2002 after OTFT process fabrication steps. AFM data collected over 10 μm area. See Figure S1 (Supporting Information) for AFM height images.

Surface Roughness [nm]	R_a [nm]	R_{ms} [nm]
SU8 as cured	0.255	0.321
SU8 after S/D patterning	0.455	0.603
SU8 + S/D + plasma	0.816	1.41

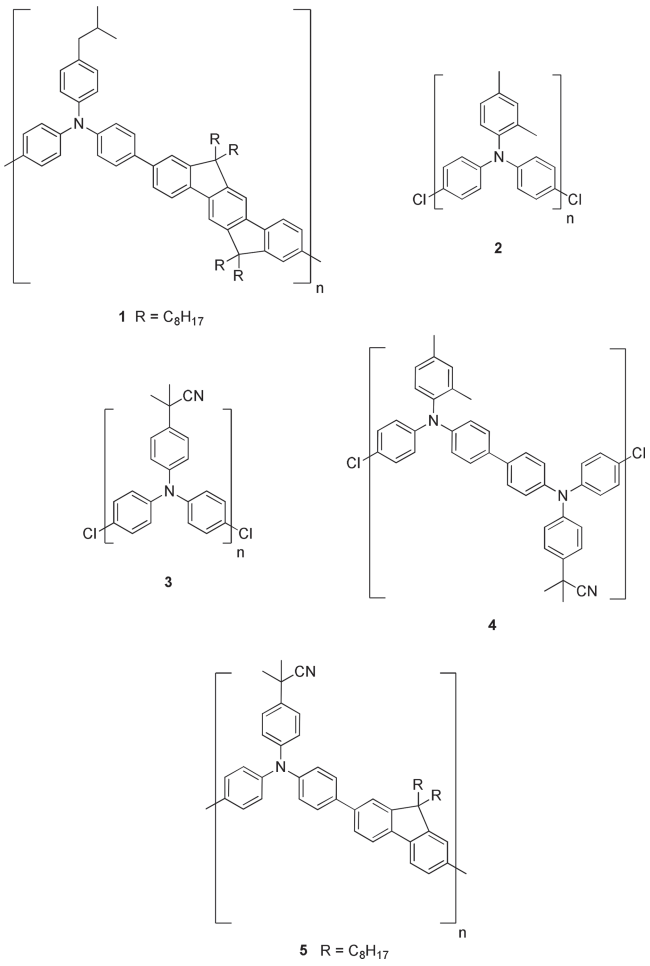

Figure 2. Chemical structures of semiconducting binder materials prepared. Details and discussion of synthesis is available in Supporting Information.

(5.9) but significantly decreased solubility in the preferred range of solvents for OSC fabrication. Thus, a series of random copolymers were prepared, containing differing proportions of 2,4-dimethyl and 4-(isopropylcyano) triarylamine monomer units. This strategy allowed "tuning" of the material permittivity, without significantly changing other key parameters such as charge carrier mobility (Table S1, Supporting Information). Furthermore, these copolymers had improved solubility compared to homopolymer **3**. Copolymer **4**, which contained 4-(isopropylcyano) and 2,4-dimethyl triarylamine monomers in a 30:70 ratio, exhibited a good balance of properties (permittivity, solubility and charge carrier mobility) and was selected for further study.

Table 3 summarizes the properties of the binders studied. As can be seen from the permittivity values for the binders, introducing polar groups to the pendant triarylamine ring results in an increased permittivity of the oligomer. This is a consequence of shifting the electron density onto the pendant ring thereby introducing a larger dipole in the polymer. This effect is however not significant enough to change the ionization potential of the material significantly. It might be expected that the inclusion of cyano groups would induce a more significant increase due to the strong electron withdrawing nature of the substituent. However it is believed that the fact that the group is not directly attached to the pendant ring means that the electronic coupling between the aromatic electrons and the CN is minimized. It should be noted that when the CN group was directly attached to the ring, the ionization potential of the polytriarylamine shifts to a significantly higher value of 5.5 eV.

The binders chosen for this study all show similar rheology due to the low molecular weight and PDI for each, and show little variation in the ionization potential, therefore any difference observed between the systems is surmised to be due to the permittivity value of the binder.

4. Results and Discussion

4.1. OTFT Performance

These binders were each formulated with TMTES, and incorporated into top-gate bottom contact OTFT arrays fabricated using SU8-2002 as a planarizing sub-layer. To allow a more accurate comparison between the binder systems, a statistically significant number of devices was tested on each array fabricated and the median mobility is presented along with the standard deviation (s.d. %). This also demonstrates the variation of performance across the array itself. A comparison of the effects of surface energy on the OSC formulation performance with different binders was made, using an argon/oxygen plasma

Table 3. Summary of binder properties.

Chemical Description of Binder	Permittivity (k)	Molecular weight (M_n)	Polydispersity (PDI)	Mobility [$cm^2 V^{-1} s^{-1}$]	Ionization Potential [eV]
4-sec butyl triarylamine/C8-Indenofluorene (4-SB-TAA/C_8-IF; 50/50 copolymer)	2.6	14150	2.0	8×10^{-3}	5.2
2,4-DiMethyl-triarylamine (2,4-DiMe-TAA homopolymer)	3.0	3150	1.8	4×10^{-3}	5.1
4-isopropylcyano-triaryalmine/2,4-dimethyl triarylamine (4-iPrCN/2,4-DiMe PTAA; 30/70 copolymer)	3.7	2000	3.4	1×10^{-4}	5.1
4-isopropylcyano triarylamine/n-octyl Fluorene (4-iPrCN TAA/C_8-Flu, 70/30 copolymer)	4.6	9700	1.8	1×10^{-5}	5.2

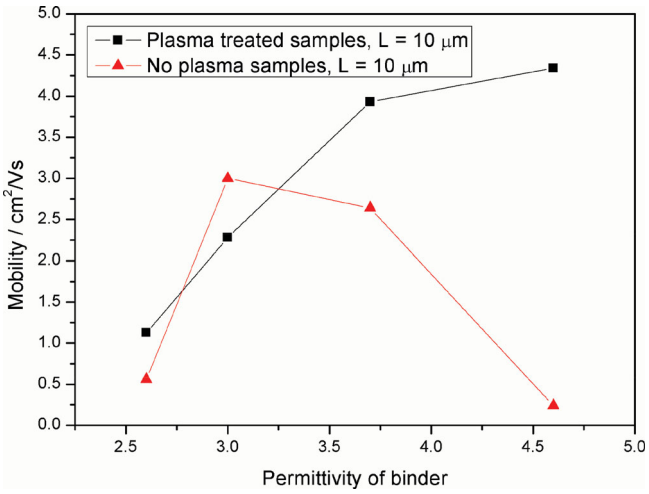

Figure 3. Variation of OTFT linear mobility at L = 10 μm with permittivity of binder used in TMTES formulation. Effect of variation of SFE also shown.

treatment of the substrate and electrodes prior to the OSC formulation coating ensuring that a polar surface was obtained. The lower surface energy sample was prepared using exactly the same processing conditions except that the plasma step was omitted prior to deposition of the OSC layer. In all cases, the film thickness of the OSC layer was ≈20 nm (measured by surface profilometry and vertical interferometry) and was shown not to be dependent on the binder used nor the SFE of the substrate.

Figure 3 and **Table 4** compare the OTFT performances for each of the binder formulations using a range of surface energies. When comparing the mobility data obtained from a plasma treated surface versus a non-plasma treated surface, the high permittivity binders show a higher dependence on the surface energy, with untreated (lower SFE) surfaces yielding significantly lower mobilities than the corresponding plasma treated (higher SFE) OTFTs, **Figure 4**. The low-k binders show limited difference between the high and low polarity surfaces and generally show a higher standard deviation of the mobilities.

When investigating the TMTES morphology for the variable permittivity binder formulations it was observed that the crystalline domain size and appearance of the grain boundaries was very similar. Optical microscopy shows no significant difference in appearance across the substrate nor between binders or SFE condition (see supporting information). The OSC layer appearance is consistently platelet type crystals with dimensions typically less than 100 μm. AFM investigation of the top surface of the OSC layer for the highest and lowest permittivity binder formulations, showed very similar platelet crystalline domains with no significant difference in grain boundaries or crystal orientation observable, **Figure 5**. The fact that the TMTES morphology is not significantly different between the films with varying binder permittivity suggests that the reason the mobilities vary between the systems is not due to significant differences at the OSC/dielectric interface but is related to the depth profile of the small molecule/binder film.

We can surmise from these results that the combination of a polar surface and a small molecule/high-k binder results in a more stable phase separation than in the case of the small molecule/low-k formulation. This technical effect should enable a wider process window to be realized in industrially relevant solution coating processes such as slot-die coating or spin coating when compared with the previously used low-k formulations. The role of phase separation with regards small molecule-polymer formulations and the resultant OTFT performance has been discussed previously.[7,8,19,20,21] The conclusions from the references combined with the observations from this study lead us to conclude that with a higher uniformity of the phase separation in the vertical direction of the film, an improved overall performance can be achieved. The cause of this improved vertical phase separation is postulated to be attributed to increased dipole-dipole interactions between the plasma treated, and therefore oxygen functional group rich, SU8-2002 planarizing layer and the high polarity high-k binders. The presence of a larger dipole in the case of the more polar high-k binders may result in a preferential higher

Table 4. Summary of OTFT characteristics for different binder formulations; TFT channel length, L = 10 μm and width, W = 1100 μm. All formulations are 1.2 wt% 1:2 small molecule:binder in tetralin.

Description of the Formulation	Binder Permittivity	Plasma Treatment	Median linear mobility [$cm^2 V^{-1} s^{-1}$]	s.d. of mobility [%]	No. of devices
TMTES only	n/a	Y	0.95	49.6	21
TMTES only	n/a	N	0.22	87.5	7
TMTES/ (4-SB-TAA/C_8-IF) (50/50 copolymer)	2.6	Y	1.13	37.2	19
TMTES /(4-SB-TAA/C_8-IF) (50/50 copolymer)	2.6	N	0.56	51.9	21
TMTES/2,4-DiMe-PTAA	3.0	Y	2.28	15.8	24
TMTES/2,4-DiMe-PTAA	3.0	N	3.00	8.6	32
TMTES/(4-iPrCN/2,4-DiMe-PTAA) (30/70 copolymer)	3.7	Y	3.93	5.2	32
TMTES/(4-iPrCN/2,4-DiMe-PTAA) (30/70 copolymer)	3.7	N	2.64	22.6	29
TMTES/(4-iPrCN-TAA/C_8-Flu) (70/30 copolymer)	4.6	Y	4.34	7.7	30
TMTES/(4-iPrCN-TAA/C_8-Flu) (70/30 copolymer)	4.6	N	0.24	30.3	27

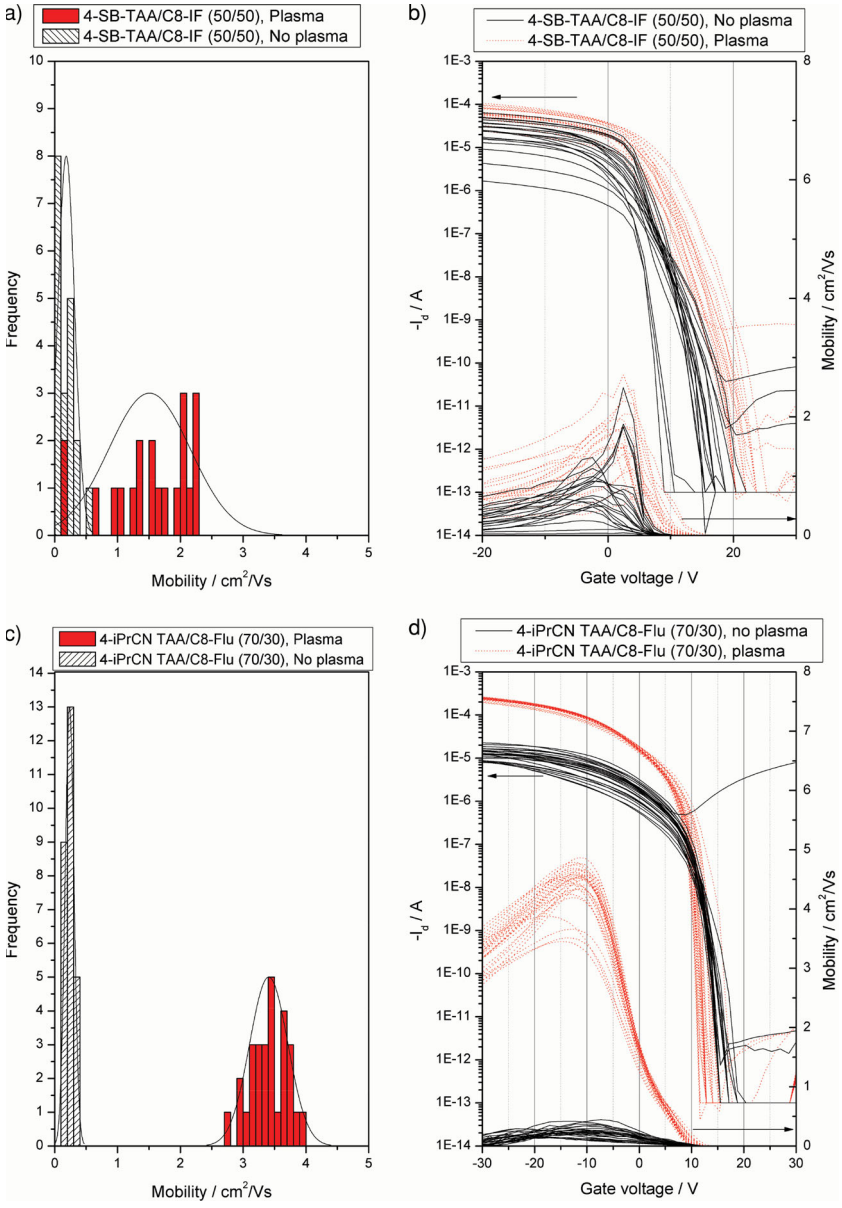

Figure 4. a) Histogram summary of mobility data for OTFTs with L = 10 µm using the low-k binder 4-SB-TAA/C8-IF (50/50 copolymer) formulated with TMTES. b) Transfer curves for 4-SB-TAA/C8-IF (50/50 copolymer) and TMTES, with variable SFE. c) Histogram summary of mobility data for 4-iPrCN-TAA/C8-Flu (30/70 copolymer) and TMTES. d) Transfer curves for 4-iPrCN-TAA/C8-Flu (30/70 copolymer) and TMTES. Further histograms and transfer curves for the full range of binders formulated with TMTES and the small molecule only data are presented in Supporting Information.

concentration of the binder polymer at the SU8-2002 interface, thereby resulting in an increased concentration of the TMTES small molecule at the air interface of the OSC thin film. The increased concentration thereby resulting in improved molecular ordering of the polycrystalline small molecule, and hence improved OTFT performance.

For comparative purposes, OTFT devices were also prepared by coating TMTES in the absence of any binder. The performance of the OTFTs across the array show significant variation and overall the mobility and uniformity of the OTFTs were appreciably poorer than when formulated with binder materials. This is most probably due to the rheology of the binder materials improving the film forming properties of the formulation and thereby resulting in a more uniform crystalline film, with improved molecular ordering of the small molecule. These results correlate well with earlier studies of solution processed small molecule only devices versus small molecule in binder formulations.[22]

4.2. Repeatability of OTFT Performance

Additionally, and as a result of the enhanced vertical phase separation due to dipolar interactions between the binder and the planariser surface, the high-k binder formulations show extremely high repeatability from substrate to substrate when a plasma treatment is used prior to OSC coating. Using the formulation with the 4-iPrCN/2,4-DiMe PTAA (30/70) binder, 15 substrates were prepared, 1 month apart from each other. **Figure 6** and **Table 5** show a histogram of mobility data taken from TFTs with channel length L = 10 µm, which yielded a median mobility of 3.3 $cm^2\ V^{-1}\ s^{-1}$ with standard deviation over this 15 month period of 8 % for the 347 devices tested. Due to the compatible chemistry of the high-k binders to the surface energy of the substrates, this leads to highly repeatable data and a resulting well-controlled process can be established. In comparison, repetition of array fabrication using a formulation with the low-k binder 2,4-DiMe-PTAA showed much poorer uniformity, when evaluating data from substrate to substrate, (refer to Table 5 and Figure 6). As demonstrated, the standard deviation for this low-k formulation show ≈20 % variation in the mobility across the substrates. This is thought to be due to the fact that the low-k binder having a permittivity of 3.0, and therefore a smaller dipole moment, is not interacting with the polar surface to the same degree as the high-k binders with larger dipoles. Therefore the phase separation of the low-k binder and small molecule will be influenced more heavily by the numerous other variables for example solvent evaporation rate or lab temperature and humidity levels. This lack of control therefore leads to more variable results across a single array of OTFTs or between different substrates. This further demonstrates the industrial usefulness of high-k binders, and when used in combination with controlled surface energy of the substrates from run to run, significant improvements in reproducibility can be achieved.

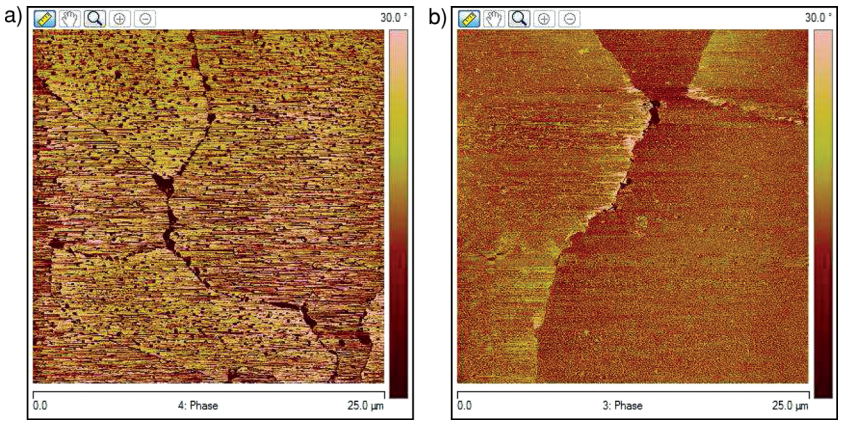

Figure 5. AFM phase images of a) TMTES/4-SB-TAA/C8-IF (50/50 copolymer) and b) TMTES/4-iPrCN TAA/C8-Flu (30/70 copolymer). Both films were prepared on SU8 substrates treated with a 50/50 sccm Ar/O_2 plasma.

4.3. Channel Length Dependence

Channel length dependence of OTFT mobility is a serious technical issue that can prevent promising OSC materials from achieving high performance in industrial processes. This is the tendency for the mobility of devices to reduce with decreasing channel length. In this work it was found that with the optimized phase separation of the high-*k* binder formulations, improved channel length dependence was achieved, relative to the low-*k* binder formulations, **Figure 7**. This optimized OSC formulation allows the demonstration of OTFT mobility at channel length of only 5 µm to be greater than 4 $cm^2\ V^{-1}\ s^{-1}$. One possible reason for the reduced channel length dependence may be due to the thin (25 nm) OSC layer. Charge transport in the amorphous binder material or through the out of plane axis of the TMTES small molecule is substantially lower than in the plane of the conducting channel and consequently a thin OSC layer will have a low bulk film resistance. In the case of a top gate device, charge carriers injected from the source electrode can reach the conducting channel easily. Producing a uniform thin OSC layer over a large area from a polycrystalline material is technically very challenging. Using binder materials, particularly the high-*k* versions, allow this film to be spin coated without film breakup, and therefore the crystalline channel material can be within the desired close vertical proximity of the electrodes.

5. Conclusion

The use of high permittivity semiconducting binders in OSC formulations has resulted in high mobility OTFTs at short channel lengths. Furthermore they allow controlled solution coating onto polar surfaces and can achieve highly reproducible, excellent uniformity OTFT arrays. This appears to be due to the increased dipole–dipole interactions between the binder and the plasma treated surface leading to significantly improved vertical phase separation of the small molecule and binder within the OSC formulation. It is therefore proposed that high-*k* binders, in combination with a high performance small molecule, can readily and repeatedly achieve very high mobility solution processed OTFTs with performance levels in excess of 4 $cm^2\ V^{-1}\ s^{-1}$ at channel lengths below 10 µm. Further work is currently ongoing in this area, investigating the phase separation differences between high-*k* and low-*k* systems using thin film depth profiling techniques.

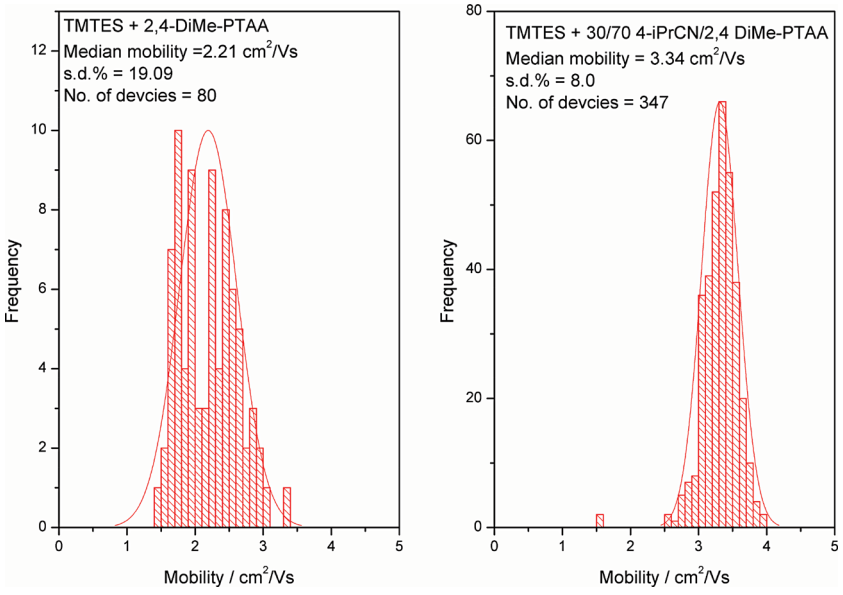

Figure 6. Histogram of mobility data for TFT having L = 10 µm, obtained from several substrates, comparing low-*k* (2,4-DiMe-PTAA) and high-*k* (4-iPrCN/2,4-DiMe-PTAA) binder repeatability.

6. Experimental Section

Material Synthesis: All oligomer and small molecule materials were prepared as previously described.[9,23,24]

SFE Measurement Method: A CAM101 goniometer (KSV Instruments) was utilized to measure contact angles of standard test liquids (di-iodomethane and high-purity water) on the surfaces under study. Surface free energy values were calculated using an OWRK / Extended Fowkes method.

AFM Method: The AFM study of the SU8 surface after various process steps was carried out using a Veeco Nanoscope V, Dimensions 3100, instrument in tapping mode, in air and ambient cleanroom conditions. 10 µm areas were investigated in separate locations across a 4 inch substrate to confirm data validity for the study of SU8 surfaces. For substrates with a source-drain pattern, the area of study was carried out between devices. OSC layers were investigated using the same technique using 25 µm areas.

Table 5. Statistical data obtained for repeat TFT fabrication using high and low-*k* binder formulations, with surface energy variation demonstrated. Data shown is from $L = 10$ µm.

Formulation	Median mobility [$cm^2 V^{-1} s^{-1}$]	s.d. of mobility [%]	No. of devices
TMTES/(iPrCN/DiMe-PTAA) (30/70 copolymer)	3.3	8.0	347
TMTES/(2,4-DiMe-PTAA)	2.2	19.1	80

Permittivity Measurement Method: 50 nm titanium bottom contact pads were prepared using sputter coating and standard photolithography and wet etching techniques. The oligomer was then spin coated from solution, to obtain a film thickness of typically greater than 500 nm. A top contact pad of approximately 50 nm aluminium was then deposited using shadow mask evaporation. The capacitance was measured using a calibrated Agilent Precision LCR meter E4980A set at a frequency of 1000 Hz. Film thickness measurements were performed using a Dektak surface profilometer and cross correlated with a Taylor Hobson Talysurf CCI white light interferometer. The two techniques were found to agree to within ±3% for all films studied. The area of overlap for the top and bottom contact pads, that is, the area of the capacitor formed, was measured using a Zeiss stereo microscope equipped with image analysis software. Using these values the permittivities were then calculated using the equation:

$$\varepsilon_r = \frac{C \cdot d}{A \cdot \varepsilon_0} \quad (1)$$

where, ε_r is the permittivity of the polytriarylamine analogue, C is the measured capacitance of the capacitor, d is the thickness of the film of the polytriarylamine analogue, A is the area of the capacitor, and ε_o is the permittivity of free space (a constant with a value of 8.854×10^{-12} F m^{-1}).

The capacitor array used contains 64 capacitors with areas of 0.11 cm^2 and 0.06 cm^2 respectively (32 of each size). The standard deviation for the value of permittivity on each array was calculated, which includes the standard deviation of capacitance, film thickness and area measurement combined. In addition, the oligomer film was tested at two different film thicknesses to confirm that the permittivity value did not vary with film thickness.

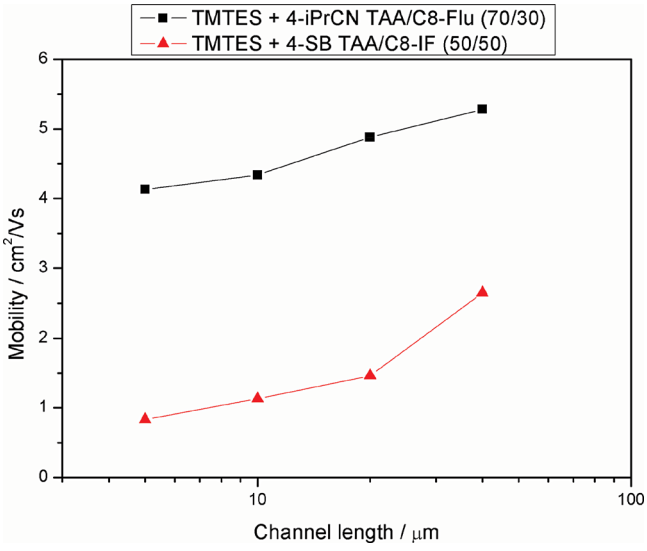

Figure 7. OTFT channel length dependence for high-*k* binder formulation (TMTES + 4-iPrCN-TAA/C_8-Flu (70/30)) and low-*k* binder formulation (TMTES + 4-SB-TAA/C_8-IF (50/50)).

Ionization Potential Measurement: Kelvin probe measurements were made using a 5 mm stainless steel tip and thin films of the binder materials on Au substrates. Each value reported is an average of 10 measurements and ionization potentials calculated were relative to 2,4-DiMe-PTAA and polyvinylcarbazole measured at the same time as the novel binder materials. Cross-correlation by Riken AC2 photoelectron spectroscopy has also been completed to validate these results.

Transistor Fabrication Method: Transistors were fabricated in top gate/bottom contact configuration using an SU8-2002 planarising layer on glass substrates. Au source and drain (S/D) electrodes were patterned using photolithography and wet etching. The S/D and gate electrodes were patterned in the corbino arrangement with channel lengths of 40, 20, 10, and 5 µm, see Figure S11 (Supporting Information). The corbino arrangement allows a high on/off ratio to be measured without the requirement of OSC isolation to eliminate parasitic currents. When required a plasma treatment of the surface was carried out using 50/50 sccm argon/oxygen plasma, 250 W, 60 s (PE100, Plasma Etch Inc.) The small molecule utilized in the OSC formulations for all binder systems was 1,4,8,11-tetramethyl-6,13-bis(triethylsilylethynyl) pentacene and was a 1.2 wt% formulation in tetralin prepared at a 1:2 ratio with the binder. The fluoropolymer Cytop CTL-809M was chosen as the dielectric due to the high degree of orthogonality between fluorosolvents and the OSC materials studied. The gate metal was evaporated Au, which was patterned using photolithography. Typical gate leakage data for an array is shown in Figure S12 (Supporting Information) and demonstrates that the integrity of the dielectric layer was excellent and uniform across the array. Any OTFT device that showed high gate leakage (i.e., $I_d/I_g < 10$ at the highest gate voltage applied in accumulation) was omitted from the statistical analysis.

OTFTs were tested using a Wentworth Pegasus 300S semi-automated probe station in conjunction with a Keithley S4200 semiconductor parameter analyser. This allowed a statistically significant number of OTFT device measurements to be made on each substrate. The Keithley system calculated the linear mobility according to

$$\mu = \frac{\delta I_{ds}}{\delta V_g} \frac{L}{W C_i V_{ds}} \quad (2)$$

where L is the transistor length, W is the transistor width, and C_i is the dielectric capacitance per unit area. V_{ds} was set at –2 V. The mobility values reported are an average of the 5 highest points from the mobility curve for each transistor. The standard deviation of the mobility values is reported as a percentage of the mean, and the number of devices measured is indicated in the table of results also.

Supporting Information

Supporting Information is available from the Wiley Online Library or from the author.

Received: September 27, 2013
Revised: November 29, 2013
Published online: February 12, 2014

[1] a) F. Arefi, V. Andre, P. Montazer-Rahmati, J. Amouroux, *Pure Appl. Chem.* **1992**, *64*, 715; b) C. Wang, H. Dong, W. Hu, Y. Liu, D. Zhu, *Chem. Rev.* **2012**, *112*, 2208.
[2] Y. Nakajima, T. Takei, T. Tsuzuki, M. Suzuki, H. Fukagawa, T. Yamamoto, S. Tokito, *J. Soc. Inf. Disp.* **2009**, *17*, 629.
[3] Y. Fujisaki, Y. Nakajima, T. Takei, H. Fukagawa, T. Yamamoto, H. Fujikake, *IEEE Trans. Electron. Devices* **2012**, *59*, 3442.
[4] a) M. P. Hong, B. S. Kim, Y. U. Lee, K. K. Song, J. H. Oh, J. H. Kim, T. Y. Choi, M. S. Ryu, K. Chung, S. Y. Lee, B. W. Koo, J. H. Shin, E. J. Jeong, L. S. Pu, *SID 05 Digest* **2005**, *36*, 23; b) S. E. Burns,

W. Reeves, B. H. Pui, K. Jacobs, S. Siddique, K. Reynolds, M. Banach, D. Barclay, K. Chalmers, N. Cousins, P. Cain, L. Dassas, M. Etchells, C. Hayton, S. Markham, A. Menon, P. Too, C. Ramsdale, J. Herod, K. Saynor, J. Watts, T. von Werne, J. Mills, C. J. Curling, H. Sirringhaus, K. Amundson, M. D. McCreary, *SID 06 Digest* **2006**, 3.
[5] K. Nomoto, *SID 10 Digest* **2010**, *41*.
[6] S. D. Ogier, J. Veres, M. Zeidan, Application: *WO Patent 2007082584* **2007**.
[7] R. Hamilton, J. Smith, S. Ogier, M. Heeney, J. E. Anthony, I. McCulloch, J. Veres, D. D. C. Bradley, T. D. Anthopoulos, *Adv. Mater.* **2009**, *21*, 1166.
[8] N. Shin, J. Kang, L. J. Richter, V. M. Prabhu, R. J. Kline, D. A. Fischer, D. M. DeLongchamp, M. F. Toney, S. K. Satija, D. J. Gundlach, B. Purushothaman, J. E. Anthony, D. Y. Yoon, *Adv. Funct. Mater.* **2013**, *23*, 366.
[9] B. A. Brown, S. D. Ogier, M. Palumbo, K. L. McCall, Application: *WO Patent 2012160383* **2012**.
[10] R. Hamilton, J. Smith, S. Ogier, M. Heeney, J. E. Anthony, I. McCulloch, J. Veres, D. D. C. Bradley, T. D. Anthopoulos, *Adv. Mater.* **2009**, *21*, 1166.
[11] Z. He, D. Li, D. K. Hensley, A. J. Rondinone, J. Chen, *Appl. Phys. Lett.* **2013**, *103*, 113301.
[12] T. Ohe, M. Kuribayashi, R. Yasuda, A. Tsuboi, K. Nomoto, K. Satori, M. Itabashi, J. Kasahara, *Appl. Phys. Lett.* **2008**, *93*, 053303.
[13] M. M. Ibrahim, A. C. Maciel, C. P. Watson, M. B. Madec, S. G. Yeates, D. M. Taylor, *Org. Electron.* **2010**, *11*, 1234.
[14] Y. Kuo, in Interface The Electrochemical Society **2011**, 55.
[15] J. A. G. Baggerman, R. J. Visser, E. J. H. Collart, *J. Appl. Phys.* **1994**, *75*, 758.
[16] P. D. F. Walther, S. Zurcher, M. Kaiser, H. Herberg, A. Gigler, R. W. Stark, *J.Microm. Microeng.* **2007**, *17*, 11.
[17] W. M. M. Heckmeier, W. Zhang, D. Sparrowe, G. Lloyd, S. Tierney, S. Derow, Application: *WO Patent 2009065479* **2009**.
[18] J. F. J. Allen, S. Leeming, J. Morgan, M. Thomas, Application: *WO Patent 1999032537* **1999**.
[19] J.-H. Kwon, S.-I. Shin, K.-H. Kim, M. J. Cho, K. N. Kim, D. H. Choi, B.-K. Ju, *Appl. Phys. Lett.* **2009**, *94*, 013506/1.
[20] Y.-H. Kim, J. E. Anthony, S. K. Park, *Org. Electron.* **2012**, *13*, 1152.
[21] J. Smith, R. Hamilton, M. Heeney, D. M. de Leeuw, E. Cantatore, J. E. Anthony, I. McCulloch, D. D. C. Bradley, T. D. Anthopoulos, *Appl. Phys. Lett.* **2008**, *93*, 253301.
[22] B. A. Brown, J. Veres, R. M. Anemian, R. T. Williams, S. D. Ogier, S. W. Leeming, Application: WO Patent 2005055248, **2005**.
[23] B. Brown, S. D. Ogier, M. Palumbo, K. L. McCall, R. Fisher, M. J. Simms, N. D. Forrest, A. J. Page, S. E. Willetts, J. D. E. Jones, Application: *WO Patent 2012160382* **2012**.
[24] G. R. Llorente, M. B. Dufourg-Madec, D. J. Crouch, R. G. Pritchard, S. Ogier, S. G. Yeates, *Chem. Commun.* **2009**, 3059.